

Design and Fabrication of a Sectoral Beam Slotted Antenna in SIW Technology for Surveillance Applications at Millimeter Waves

Santi C. Pavone^{1, *} and Matteo Albani²

Abstract—In this paper, we present the design and fabrication of a sectoral beam slotted antenna in substrate integrated waveguide (SIW) technology able to achieve a high roll-off sectoral pattern in the horizontal plane and a very narrow beam in the vertical plane, as required in surveillance applications in the band 76–77 GHz. The proposed antenna is designed and fabricated in multi-layer PCB technology, which allows to integrate both the corporate feeding network and the radiating aperture in the same planar and lightweight device. To achieve a remarkable roll-off (> 5.5 dB/deg) and a reduced ripple (< 1.5 dB), the antenna has been designed by synthesizing a *sinc*-shaped (uniform) aperture distribution along x -direction (y -direction). The synthesis and optimization of so tapered aperture distributions is not easy to be found in the literature, especially for planar devices. A prototype of such an antenna has been fabricated with a horizontal half-power beamwidth (HPBW) of 30° , by embedding both the feeding network and the radiating aperture in three stacked dielectric substrates. Measurements of the prototype show a fair agreement with numerical simulations.

1. INTRODUCTION

Substrate integrated waveguides (SIWs) can be considered nowadays an enabling technology that allows to design compact and relatively low-cost planar electromagnetic devices at microwaves and millimeter waves, both for antennas [1–5] and waveguide applications [6–9]. Indeed, SIWs can be profitably adopted to design several microwave devices such as filters, splitters, junctions, and cavities, only to mention a few, thanks to their compactness and manufacturing easiness. They simply consist of two rows of suitably designed metallic pins behaving as equivalent electric walls. Such pins are electrically connected to the substrate top and bottom metal planes, thus allowing SIWs to efficiently guide an incoming electromagnetic field [6].

In the last decade, SIWs started representing a valid alternative to more standard rectangular waveguides for low-power applications at millimeter waves, since they can be profitably integrated and manufactured in PCB technology, whereas rectangular waveguides are usually heavier devices and require expensive mechanical processes to be fabricated with high accuracy. Their compactness can also pave the way for novel lightweight scanning antenna solutions, based on reconfigurable metasurfaces [10]. On the other hand, SIWs can be considered a good candidate for designing both traveling-wave and standing-wave slotted antenna arrays at millimeter waves, since slots can be readily etched on SIWs, by making use of mature technologies for printed circuits, such as photolithography. Hence, most of the techniques developed in the last years for the synthesis of almost arbitrary aperture field distributions in planar slotted devices, such as for instance radial-line slot-arrays (RLSA) for both antenna [11–15] and focusing [16–20] applications, can be suitably applied also to SIW devices.

Received 21 January 2020, Accepted 26 April 2020, Scheduled 31 May 2020

* Corresponding author: Santi Concetto Pavone (santi.pavone@unict.it).

¹ Department of Electrical, Electronics and Computer Engineering (DIEEI), University of Catania, Viale Andrea Doria 6, Catania 95125, Italy. ² Department of Information Engineering and Mathematics (DIISM), University of Siena, Via Roma 56, Siena 53100, Italy.

The state of art of antennas radiating a sectoral pattern presents only few examples of antennas in compact planar multilayer technology, since in general *sinc*-shaped or tapered aperture distributions are synthesized by means of horn arrays [21], horn antennas with shaped dielectric lenses [21–23] or EBG structures [24], and commonly reflector systems [25]. Instead, in this paper, we propose the design and optimization of a sectoral beam standing-wave slotted antenna array for surveillance applications at 76.5 GHz, following the systematic procedure explained in detail in [26] and profitably used in [27–29]. It is worth noting that the proposed antenna has been fabricated by using the PCB technology normally adopted in electronics, hence it is planar, relatively low-cost, very compact and lightweight. Moreover, PCB technology allows to design and fabricate multi-layer devices, which can integrate both the feeding network and the radiating aperture.

A rectangular aperture distribution has been properly optimized to radiate a narrow pattern in the vertical plane and a sectoral pattern in the horizontal plane. Indeed, in surveillance applications the roll-off (RO), i.e., the pattern slope in correspondence of the transition between illuminated and non-illuminated angular regions in the horizontal plane, should be the highest possible, in order to reduce the probability of object false detection in the controlled angular sector [21]. In addition, also the ripple in the lit region has to be accurately limited, in order to provide an accurate size estimation of an object lying in the area under surveillance. The specific requirements in terms of RO and ripple have to be evaluated by considering the maximum sensibility in obstacle size detection.

It is worth noting that the sectoral pattern in the horizontal plane has been obtained by properly designing a standing-wave slotted array in SIW (i.e., a radiating row), in such a way to synthesize a truncated *sinc*-shaped aperture distribution along x -direction. On the other hand, the narrow pattern has been obtained by simply replicating the optimized rows along y -direction, in order to synthesize an uniform magnetic aperture distribution.

The paper is organized as follows. In Section 2, the antenna architecture and details on the technology used for the design are presented. In Section 3, the design criteria for the radiating aperture are provided, whereas in Section 4 the antenna corporate feeding network, used to enlarge the operating bandwidth, is discussed. Moreover, in Section 5 the fabricated prototype is shown together with impedance bandwidth and gain pattern measurements at the operating frequency. Finally, conclusions are drawn.

2. ANTENNA ARCHITECTURE AND TECHNOLOGICAL DETAILS

In this Section, the operating principles of the proposed antenna, together with the criteria adopted for its design and fabrication, are summarized. As a general remark, the antenna dimensions that are $A \times B = 70 \text{ mm} \times 100 \text{ mm}$ have been imposed by design. Moreover, the antenna has been designed by adopting the standard PCB technology, which easily allows to etch slots on laminates with high-precision (tolerance of 50–70 μm) and to make vias (tolerance on pin radii of 100 μm) required for designing SIWs. Moreover, three low-loss dielectric laminates (ROGERS 5880, $\epsilon_r = 2.2$, $\tan \delta = 9 \times 10^{-4}$) have been used to embed both the radiating aperture and the feeding network on the same compact structure. After having made slots and vias on each substrate separately, the substrates have been stacked and annealed, by interposing a high-conductivity solder paste between adjacent metallic layers. In Fig. 1(a), the stack-up of the adopted technology is sketched, in which the four metal layers, on which coupling and radiating rectangular slots, are denoted from M1 to M4, whereas the three stacked low-loss dielectric substrates, in which the vias are made to realize SIWs, are named from D1 to D3. It is worth mentioning that two laminates have been used to realize the feeding network (D1 and D2), whereas the substrate D3 hosts the radiating aperture. In Table 1, all the stack-up parameters are detailed. It should be noticed that also the optimal SIW parameters are provided at the operating frequency $f = 76.5 \text{ GHz}$, namely a_e (SIW width), T_p (post spacing) and d_p (post diameter). Such values have been determined by using the systematic procedure described in [6]. Such an approach allows to minimize losses and to prevent the excitation of higher-order modes inside the waveguides. The SIWs have simulated full-wave by considering the design parameters provided in Table 1 to evaluate the guided propagation constant β_g , which is equal to 1855 rad/m (corresponding to a guided wavelength $\lambda_g = 2\pi/\beta_g = 3.4 \text{ mm}$) at the operating frequency.

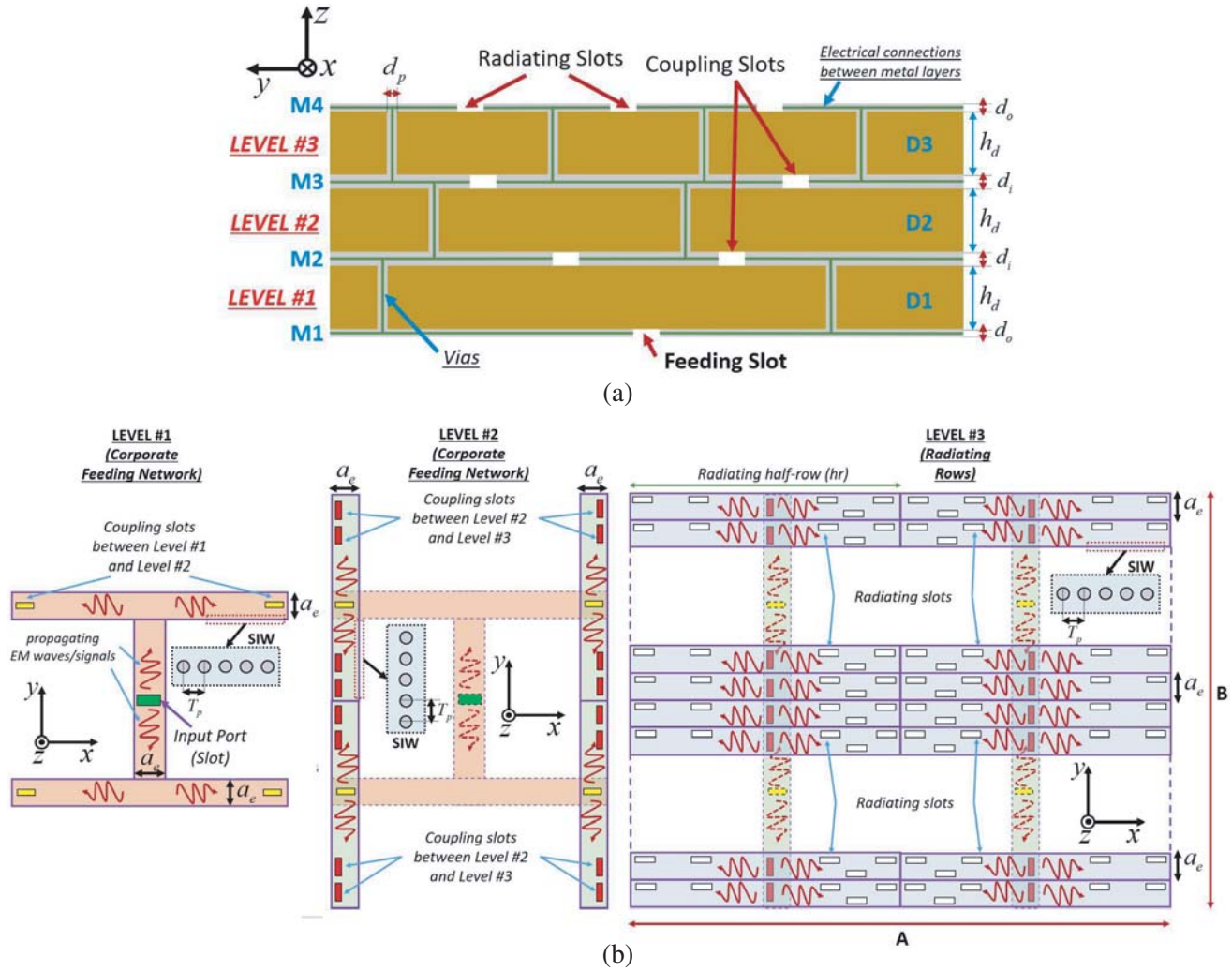


Figure 1. (a) Pictorial schematic stack-up of the multilayer SIW technology adopted to integrate both the feeding network and the radiating aperture. Three low-loss double-side laminate dielectrics, (called for simplicity D1, D2, and D3), have been stacked by annealing and soldering the metal sheets denoted by M2 and M3. (b) General architecture of the SIW designed in the dielectric layer denoted by D1 (level #1), in which an H-shaped corporate feeding network has been realized, in order to feed separately four sub-arrays. The H-shaped SIW is coupled to those in D2 (level #2) through four yellow rectangular slots (etched on M2), whereas the red slots in the broad side of the SIWs at level #2 are etched on M3. They allow to couple level #2 to the SIWs realized in D3 (level #3), which allow the radiating white slots to radiate a *sinc*-shaped magnetic current distribution.

In Fig. 1(b), the antenna general architecture is described in detail, by highlighting the three different levels in which both the corporate feeding network and the radiating aperture have been integrated. It is worth mentioning that the H-shaped SIW at level #1 has been realized in the dielectric substrate D1, whereas the four SIWs at level #2 in D2. Finally, the SIWs associated to radiating rows have been realized in D3. At level #1, the feeding wave at the input port is equally split in two waves, which excite four coupling slots (i.e., highlighted in yellow color), through the H-shaped SIW. Such (yellow) slots couple levels #1 and #2. Then, at level #2, the eight resulting waves properly feed four linear arrays of additional coupling slots (i.e., highlighted in red color), which in turn excite the radiating rows at level #3. In the following the radiating aperture and the feeding network designs will be discussed separately.

Table 1. Antenna stack-up and SIW parameters.

Parameter	Value [mm]	Description
h_d	0.79	Dielectric thickness (ROGERS 5880)
d_o	0.15	Outer metal sheet thickness
d_i	0.07	Inner metal sheet thickness
d_p	0.30	Post diameter
T_p	0.60	Post spacing (period)
a_e	2.3	SIW width

3. RADIATING APERTURE DESIGN

The proposed antenna requires to radiate a narrow (sectoral) beam in the vertical (horizontal) plane, hence a suitable equivalent magnetic current distribution to radiate such a pattern has to be shaped as a truncated *sinc*-shaped distribution in the x -direction, and as an uniform distribution in the orthogonal y -direction, namely

$$\mathbf{M}(x, y) = \frac{\sin(k \sin \theta_0 x)}{k \sin \theta_0 x} \Pi\left(\frac{x}{A}\right) \Pi\left(\frac{y}{B}\right) \hat{\mathbf{x}}, \quad (1)$$

in which k is the free-space wavenumber; A and B denote the rectangular aperture dimensions; $\theta_0 = 15^\circ$ is the -3 dB angle of the antenna pattern, whereas $\Pi(x) = 1$ for $|x| < 1/2$ and zero elsewhere (rectangular function). According to [30] and to the basic properties of spatial Fourier Transform, a pure rectangular pattern in the cut-plane at $\phi = 0^\circ$ cannot be radiated by a truncated *sinc* distribution, since the truncation due to the aperture finiteness results in a radiated pattern with a finite RO and ripple in the lit region, which is the so-called Gibbs phenomenon. For this reason, an appropriate trade-off between acceptable ripple in the lit region and high RO has to be found. The target application of the proposed antenna is the so-called medium-range surveillance (e.g., for level-crossing monitoring), in which the monitored area is approximately 20–30 m from the antenna, in a fixed angular sector (in our case, HPBW = 30°). Moreover, the imposed spatial resolution for obstacle detection is 0.5 m, as usually required for level-crossing monitoring. For such an application, a RO > 3.5 dB/deg and a ripple less than 1.5 dB can be considered acceptable [21].

The truncated *sinc* aperture distribution has been synthesized by optimizing a standing-wave slotted array [26] in SIW technology in x -direction, whereas the uniform distribution along y -direction has been achieved by simply replicating the radiating rows. To simplify and speed-up the optimization algorithm of the entire radiating rows, antenna symmetry with respect to xz -plane has been exploited. In particular, the entire radiating row has been split in two half-rows, and in turn the algorithm for optimizing slot lengths and offsets has been applied only on an half-row, in such a way to synthesize the equivalent magnetic current distribution

$$\mathbf{M}_{hr}(x) = \frac{\sin(k \sin \theta_0 x)}{k \sin \theta_0 x} \Pi\left(\frac{x - A/4}{A/2}\right) \Pi\left(\frac{y}{T_r}\right) \hat{\mathbf{x}}, \quad (2)$$

with $T_r = \lambda_g$ being the spacing between adjacent rows. To take into account the unavoidable coupling between different radiating rows, in the electromagnetic model a magnetic wall (H-wall) has been placed in the xz -plane at $y = 0$, whereas periodic boundary conditions (BCs) were considered in the yz -plane at $x = \pm T_r/2$, as shown in Fig. 2.

Then, the radiating half-rows have been optimized by considering the general approach developed by Elliott in [26], according to which rectangular slots in the broad wall of a rectangular waveguide can be circuitally represented as normalized shunt admittances $y_i = g_i + jb_i$ ($i = 1, \dots, N_s$, being N_s the number of slots in an half-row). The real part of y_i (i.e., the conductance g_i) can be increased (decreased) by increasing (decreasing) slot offsets O_i with respect to the waveguide center line, whereas the imaginary part of y_i (i.e., the susceptance b_i) can be increased (decreased) by reducing (enlarging) slot lengths L_i . A numerical optimization loop has been developed in-house and interfaced with a commercial

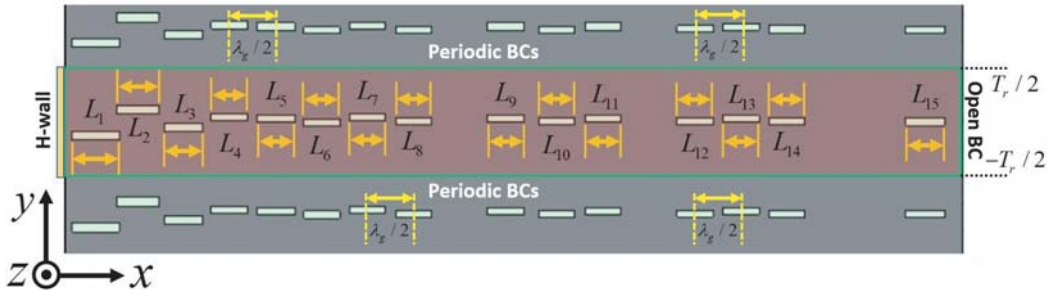


Figure 2. Geometric details of the radiating half-row, in which the slots are etched on the metal layer M4, with reference to Fig. 1. Such a slot arrangement synthesizes a *sinc*-shaped magnetic current distribution, in order to radiate a sectoral pattern in the horizontal plane. It is worth mentioning that entire radiating rows have been obtained by simply exploiting antenna symmetry with respect to xz -plane.

electromagnetic full-wave solver to fit the actual aperture distribution to the target truncated *sinc*-shaped distribution in Eq. (2), by defining suitable functionals updated at each iteration step, depending on slot lengths L_i and offsets O_i [15]. For simplicity, slot widths W_i have been linked to their lengths L_i by the aspect ratio relation $W_i = L_i/5.5$, which allows us to use a simplified slot model according to which slots can be schematized as equivalent magnetic currents dominantly oriented along slot length directions. Such an approach is very fast and allows to easily obtain the optimal slot configuration to synthesize the magnetic current distribution in Eq. (2).

The single radiating row design and optimization, obtained by considering the boundary conditions summarized in Fig. 2, has been achieved by using an in-house Matlab code, which implements the procedure outlined in the pioneering works by Elliott on standing-wave slotted array optimization. Such a code has been directly interfaced with the full-wave electromagnetic simulator CST Microwave Studio. The overall optimization process, which allows to synthesize a sampled *sinc*-like equivalent magnetic current distribution by varying slot lengths and offsets [26], is very fast, since it converges approximately after 15–20 simulation runs. Each simulation is not time-consuming (few minutes per run), since the adaptive mesh usually does not exceed 80 thousand tetrahedrons.

In Table 2 the optimal parameters for a radiating half-row are presented. Finally, in Fig. 3(a), the final aperture is shown, in which slot etched on M4 (vias made on D3) are indicated by filled rectangles (circles).

Table 2. Single radiating half-row geometric parameters after optimization.

Slot #	L_i [mm]	O_i [mm]	W_i [mm]	Slot #	L_i [mm]	O_i [mm]	W_i [mm]
1	1.72	-0.56	0.31	9	1.37	0.05	0.25
2	1.56	0.38	0.28	10	1.33	-0.06	0.24
3	1.42	-0.27	0.26	11	1.33	0.05	0.24
4	1.35	0.09	0.25	12	1.34	-0.04	0.24
5	1.42	0.04	0.26	13	1.34	0.04	0.24
6	1.33	-0.09	0.24	14	1.33	-0.05	0.24
7	1.31	0.09	0.24	15	1.42	-0.06	0.26
8	1.34	-0.06	0.24				

4. FEEDING NETWORK DESIGN

To enlarge the antenna operating bandwidth, the radiating aperture has been divided in four independent subarrays and fed by means of a corporate feeding network, as schematically depicted in

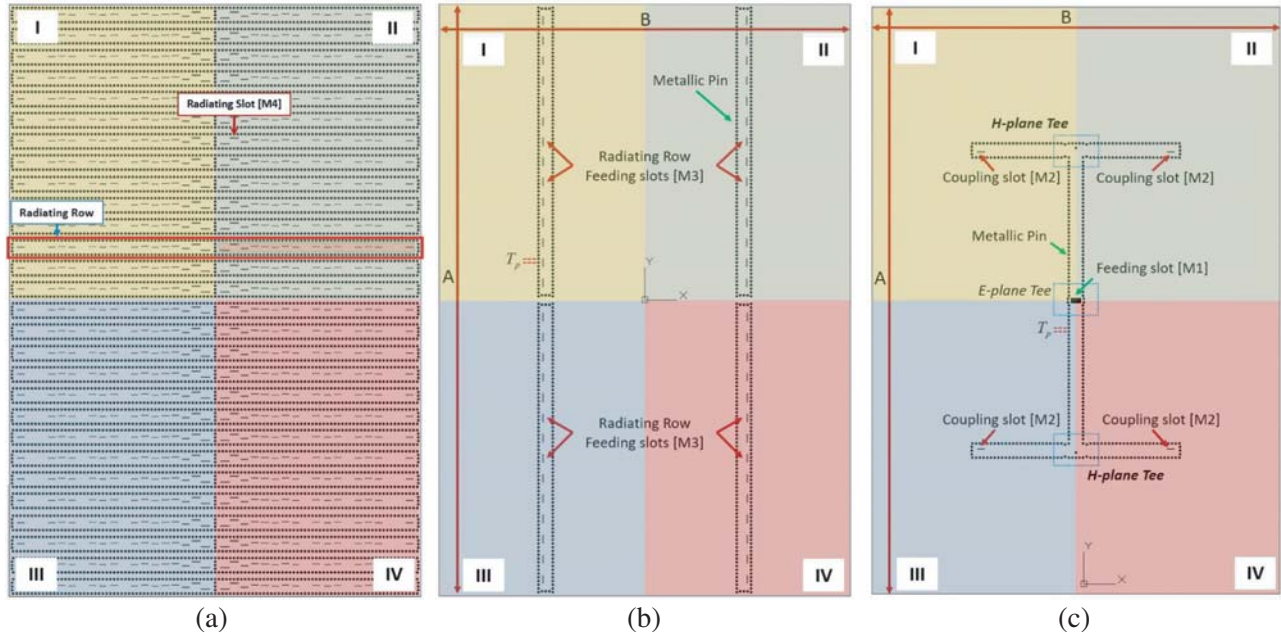


Figure 3. Antenna final architecture: drill (filled circles) and slot (filled rectangles) maps corresponding to the three different layers, namely (a) D3, (b) D2, and (c) D1, with reference to the stack-up shown in Fig. 1. The radiating aperture (feeding network) has been designed in D3 (D2 and D1). The four subarrays are denoted by I, II, III and IV.

Fig. 3. It has been designed on the dielectric substrates denoted by D3 and D2 in Fig. 1. The antenna input port is directly connected to a standard WR12 waveguide, which is the RADAR interface. With reference to Figs. 3(a)–(b), it is apparent that the radiating half-rows are fed by transverse feeding slots etched on the metal layer M3. In turn, such slots are spaced λ_g apart from each other, and placed on the maxima of the voltage standing-wave generated inside the four feeding SIWs, in such a way to excite all the slots in-phase and to maximize power transfer between D2 and D3. The feeding slots in Fig. 3(b) are then efficiently coupled to D1 through the four coupling slots etched on M2. Finally, the four waves are combined in-phase through the H-shaped SIW network depicted in Fig. 3(c) up to the antenna input port, which is a feeding slot etched on M1. It is worth mentioning that in the H-shaped SIW

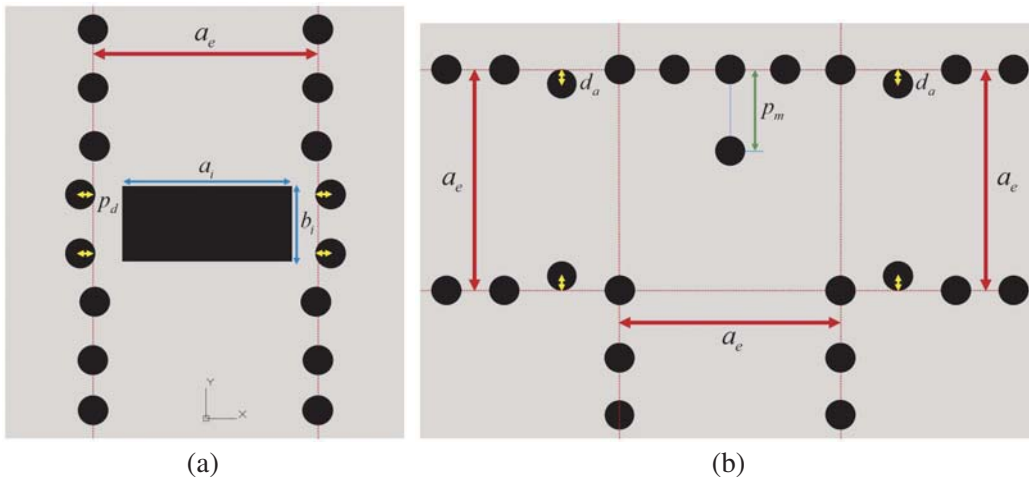


Figure 4. Geometric details of optimized (a) *E*-plane and (b) *H*-plane Tees.

network two discontinuities are present, namely two Tees in both H -plane and E -plane. To guarantee the maximum power transfer to the upper layers, they had to be properly matched at their input ports. The relevant geometric parameters to be optimized are shown in Figs. 4(a)–(b), for both E -plane and H -plane Tees. For the sake of completeness, in Table 3, the optimized parameters are presented.

The designed feeding network has been simulated together with the radiating aperture by using the full-wave frequency-domain solver of CST Microwave Studio. The computational resources used for entire full-wave simulation are non-negligible, since more than 800 thousand tetrahedrons are required (required time: 15 minutes by using an Intel Core i7, 8th generation, with a CPU working at 2.2 GHz, 16 GB RAM). Such a simulation has to run only few times, for geometry final refinements and not for the optimization of the radiating aperture. Hence, the proposed two-step optimization (i.e., radiating aperture and then feeding network) has been successful and allowed to avoid computational issues.

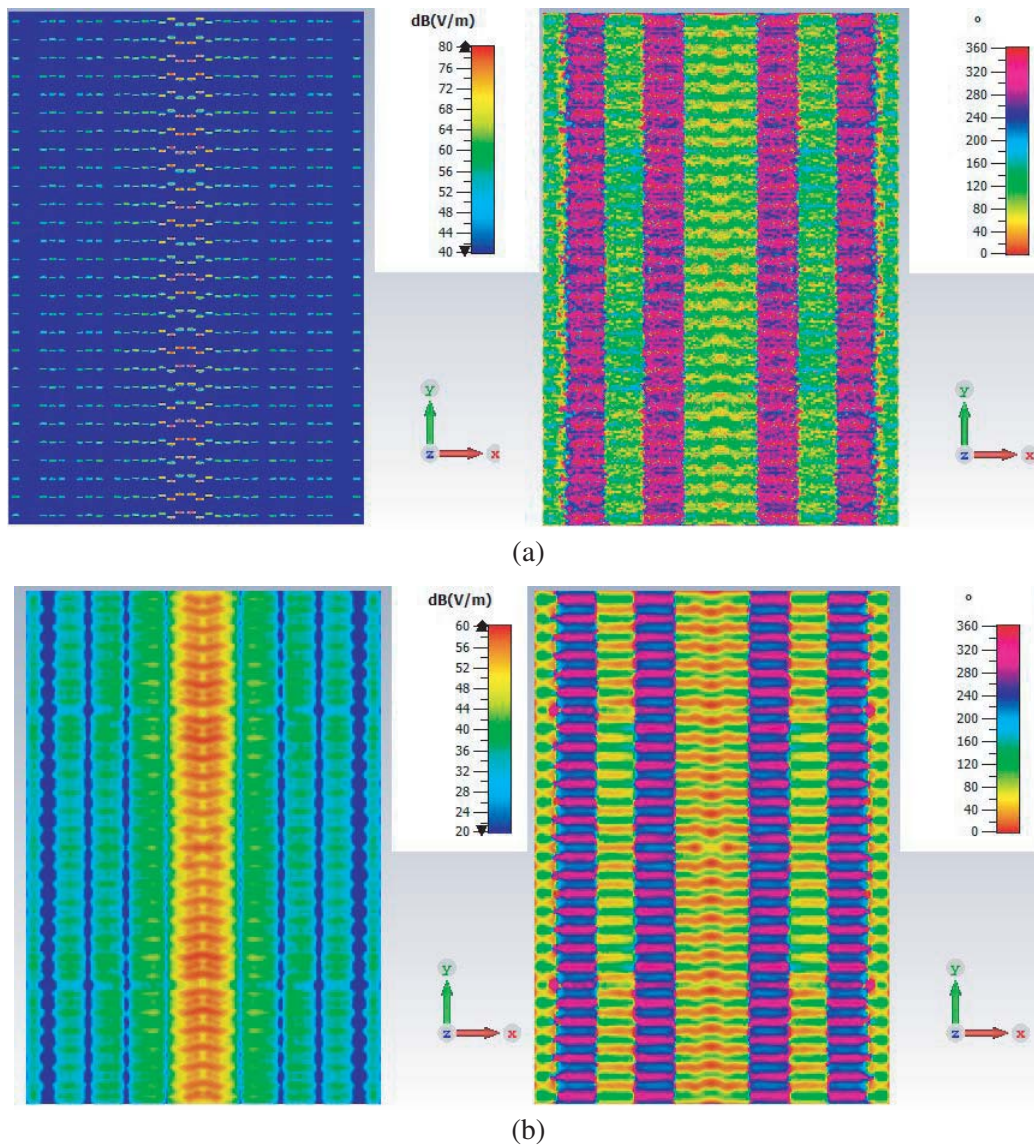


Figure 5. (a) Magnitude (on the left) and phase (on the right) of tangential electric field distribution on antenna aperture, after the optimization process. (b) Magnitude (on the left) and phase (on the right) of tangential electric field distribution at $\lambda/2$ from antenna aperture, after the optimization process. A *sinc*-shaped (uniform) profile is present along x-direction (y -direction), as required.

Table 3. E -plane and H -plane Tees optimized parameters.

Parameter	Value [mm]	Description
p_m	0.85	(H -plane Tee) Central pin displacement
d_a	0.15	(H -plane Tee) Lateral pin displacement
p_d	0.12	(E -plane Tee) Lateral pin displacement
a_i	2.06	(E -plane Tee) Iris length
b_i	1.09	(E -plane Tee) Iris width
a_e	2.30	SIW width

As a final remark, in Fig. 5(a) the magnitude (on the left) and phase (on the right) of tangential electric field distribution on antenna aperture are shown after the optimization process. For the sake of completeness and to better highlight the field amplitude distribution, in Fig. 5(b) the tangential electric field distribution is provided also at $\lambda/2$ from the radiating aperture. A *sinc*-shaped (uniform) profile is present along x -direction (y -direction), as required by design.

5. ANTENNA MEASUREMENTS

A prototype of antenna for surveillance applications at millimeter waves in SIW technology has been fabricated and measured at $f = 76.5$ GHz, following the design criteria discussed in detail in the previous Sections. In Fig. 6(a) the fabricated antenna is shown. As outlined in Table 1, three low-loss laminates have been used as dielectrics D1, D2, and D3 (ROGERS 5880, electrical permittivity $\epsilon_r = 2.2$, loss tangent $\tan \delta = 0.009$).

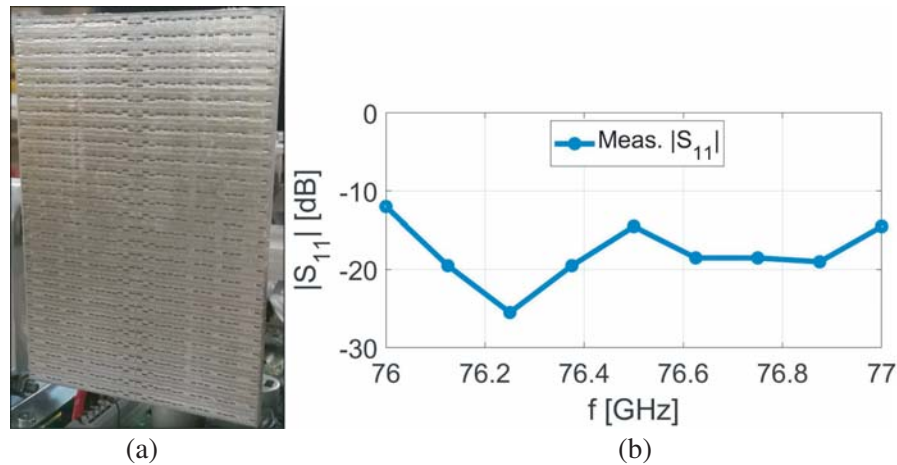


Figure 6. (a) Prototype of sectoral beam slotted antenna operating at the frequency $f = 76.5$ GHz, and (b) measured reflection coefficient at the antenna input port. The antenna exhibits $|S_{11}| < -10$ dB over all the considered bandwidth 76–77 GHz.

The measured S_{11} parameter at the input of the WR12 used to feed the antenna is quite satisfactory and demonstrates a good impedance matching, since $|S_{11}| < -10$ dB over all the bandwidth 76–77 GHz, as shown in Fig. 6(b).

Since the proposed sectoral beam antenna has been designed for surveillance applications, appropriate gain measurements on the prototype have been made. In particular, in Fig. 7(a), the adopted measurement setup is schematically shown. The antenna under test (AUT) has been mounted on a spinning table, and a metallic trihedron has been placed in a fixed position at a distance $D_{ff} \approx 10$ m

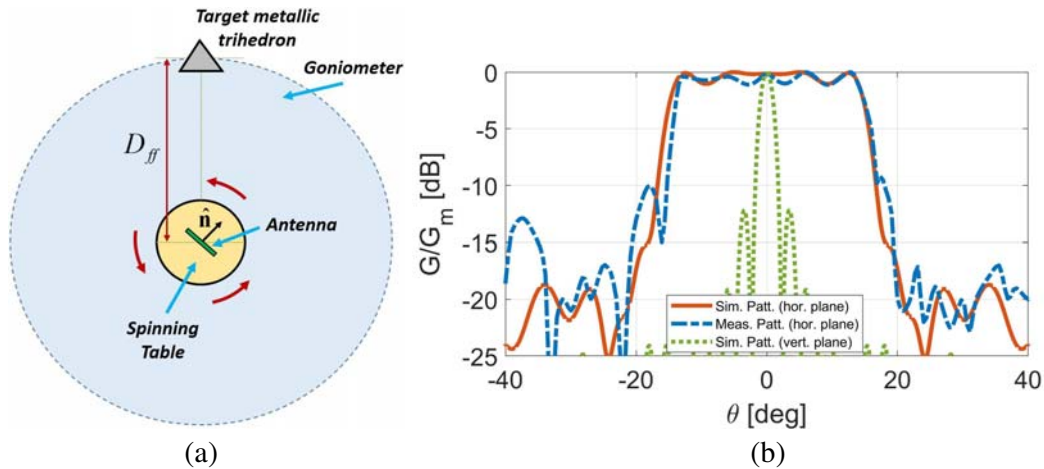


Figure 7. (a) Measurement setup for antenna azimuthal gain determination. (b) Simulated (blue dashed line) and measured (red continuous line) normalized gain patterns in the horizontal plane, and simulated (green dotted line) normalized gain pattern in the vertical plane, at $f = 76.5$ GHz.

(i.e., in the AUT far-field region). By feeding the AUT and by simultaneously rotating the spinning table, the scattered signal by the trihedron has been detected and stored. In such a way, the AUT azimuthal pattern has been determined. Moreover, to calculate AUT maximum gain G_{\max} , same measurements have been made by replacing the AUT by a standard gain antenna. By comparing results, AUT maximum gain has been calculated.

To summarize, gain measurements at $f = 76.5$ GHz revealed good pattern agreement with simulations, as apparent from Fig. 7(b), and a maximum gain of $G_{\max} \approx 20$ dB, acceptable for the target medium-range surveillance application. It should be noticed that the measured RO is remarkable, since it is higher than 5.5 dB/deg, and also the ripple in the lit region is 1.3 dB is satisfactory. Indeed, by comparing such achieved results with other different technological solutions reported in [21], it is apparent that the maximum achieved RO does not exceed in any case 3.5 dB. Such a remarkable RO allows to reduce dramatically the probability of false negative detection of obstacles that are present in the uncertainty region between lit and shadow regions. Moreover, for the sake of completeness, in Fig. 7(b) also the simulated normalized gain pattern in the vertical plane has been provided. As it is apparent, a very narrow sinc-shaped beam is radiated in the vertical plane (HPBW $\approx 2^\circ$), as required for the target application. Such a result can also be inferred from the tangential electric field distribution provided in Fig. 5, which is almost uniform in the vertical plane by design, hence the antenna radiates a narrow sinc-shaped pattern in the vertical plane. By using the antenna measurement setup already described in Fig. 7(a), the target metallic trihedron has been moved also of few degrees in the vertical plane (both at positive and negative angles), in order to prove that the simulated gain effectively decreases, as theoretically required. The results obtained have shown a fair agreement with the simulated ones.

The antenna radiation efficiency has also been evaluated in simulation for the proposed design. By stimulating the antenna with an incident power $P_{inc} = 0.5$ W, the accepted power has been proven to be very high, $P_{acc} = 0.49$ W, thanks to the very good antenna input matching. Moreover, inside the feeding network, $P_{diel} = 0.11$ W are dissipated due to dielectric losses, and $P_{met} = 0.07$ W due to copper finite conductivity. Finally, the radiated-to-accepted power is $P_{rad} = 0.31$ W, corresponding to a radiation efficiency $\eta_{rad} \approx 64\%$. Since the antenna feeding network is quite involved and integrated inside a very compact and multi-layer lossy dielectric host, such a value for antenna radiation efficiency, although not so high, can be considered quite satisfactory. Hence, such results allow the antenna to be profitably used for surveillance applications at millimeter waves.

6. CONCLUSION

We present the design and fabrication of a sectoral beam slotted antenna in SIW technology, which radiates a sectoral pattern in the horizontal plane characterized by a high RO (> 5.5 dB/deg) and a limited ripple (< 1.3 dB) in the main beam, suitable for certain surveillance applications at millimeter waves. One of the strong points of the adopted technology is the possibility of embedding both the feeding network and radiating aperture on the same compact device. A prototype has been shown with an HPBW in the horizontal plane of 30° . Pattern measurements at the operating frequency show a fair agreement with numerical simulations, and the impedance matching at the input port is satisfactory.

ACKNOWLEDGMENT

This work has been supported by the project SINATRA, an ATTRACT project which has been financed by the European Union Horizon 2020 Research and Innovation program, under grant agreement No. 777222. The Authors would like to thank Alessandro Agostini of ECM S.p.A., Serravalle Pistoiese (Pistoia, Italy), for fruitful discussions and prototype measurements, and Alberto Zanella of ESSETI Circuiti Stampati S.r.l., Argelato (Bologna, Italy), for prototype manufacturing.

REFERENCES

1. Bozzi, M., S. A. Winkler, and K. Wu, "Broadband and compact ridge Substrate Integrated Waveguides," *IET Microw. Antennas Propag.*, Vol. 4, No. 11, 1965–1973, 2010.
2. Bozzi, M., A. Georgiadis, and K. Wu, "Review of substrate-integrated waveguide circuits and antennas," *IET Microw. Antennas Propag.*, Vol. 5, No. 8, 909–920, 2011.
3. Ettorre, M., R. Sauleau, and L. Le Coq, "Multi-beam multi-layer leaky-wave SIW pillbox antenna for millimeter-wave applications," *IEEE Trans. Antennas Propag.*, Vol. 59, No. 4, 1093–1100, 2011.
4. Tekkouk, K., M. Ettorre, L. Le Coq, and R. Sauleau, "SIW pillbox antenna for monopulse radar applications," *IEEE Trans. Antennas Propag.*, Vol. 63, No. 9, 3918–3927, 2015.
5. Lyu, Y., X. Liu, D. Erni, Q. Wu, et al., "Leaky-wave antennas based on noncutoff substrate integrated waveguide supporting beam scanning from backward to forward," *IEEE Trans. Antennas Propag.*, Vol. 64, No. 6, 2155–2164, 2016.
6. Deslandes, D. and K. Wu, "Accurate modeling, wave mechanisms, and design considerations of a substrate integrated waveguide," *IEEE Trans. Microw. Theory Tech.*, Vol. 54, No. 6, 2516–2526, 2006.
7. Bozzi, M., D. Deslandes, P. Arcioni, L. Perregrini, K. Wu, and G. Conciauro, "Efficient analysis and experimental verification of substrate-integrated slab waveguides for wideband microwave applications," *Intern. Journ. RF Microw.*, Vol. 15, No. 3, 296–306, 2005.
8. Bozzi, M., L. Perregrini, and K. Wu, "Modeling of conductor, dielectric, and radiation losses in substrate integrated waveguide by the boundary integral-resonant mode expansion method," *IEEE Trans. Antennas Propag.*, Vol. 56, No. 12, 3153–3161, 2008.
9. Chu, P., W. Hong, M. Tuo, K. Zheng, et al., "Dual-mode substrate integrated waveguide filter with flexible response," *IEEE Trans. Microwave Theory Tech.*, Vol. 65, No. 3, 824–830, 2017.
10. Pavone, S. C., E. Martini, M. Albani, S. Maci, et al., "A novel approach to low profile scanning antenna design using reconfigurable metasurfaces," *2014 Intern. Radar Conf.*, 1–4, 2014.
11. Albani, M., G. La Cono, R. Gardelli, and A. Freni, "An efficient full-wave method of moments analysis for RLSA antennas," *IEEE Trans. Anten. Propag.*, Vol. 54, No. 8, 2326–2336, 2006.
12. Albani, M., A. Mazzinghi, and A. Freni, "Automatic design of CP-RLSA antennas," *IEEE Trans. Anten. Propag.*, Vol. 60, 5538–5547, 2012.
13. Montisci, G., M. Musa, and G. Mazzarella, "Waveguide slot antennas for circularly polarized radiated field," *IEEE Trans. Antennas Propag.*, Vol. 52, No. 2, 619–623, 2004.

14. Tamayo-Dominguez, A., J. Fernandez-Gonzalez, and M. Sierra Castaner, "Low-cost millimeter-wave antenna with simultaneous sum and difference patterns for 5G point-to-point communications," *IEEE Comm. Magaz.*, Vol. 56, No. 7, 28–34, 2018.
15. Pavone, S. C., M. Casaletti, and M. Albani, "Automatic design of a CP fan-beam linear slotted array in SIW technology," *IEEE Access*, Vol. 17, 155977–155985, 2019.
16. Mazinghi, A., M. Balma, D. Devona, G. Guarnieri, G. Mauriello, M. Albani, and A. Freni, "Large depth of field pseudo-Bessel beam generation with a RLSA antenna," *IEEE Trans. Anten. Propag.*, Vol. 62, 3911–3919, 2014.
17. Pavone, S. C., M. Ettorre, M. Casaletti, and M. Albani, "Transverse circular-polarized Bessel beam generation by inward cylindrical aperture distribution," *Opt. Expr.*, Vol. 24, No. 10, 11103–11111, 2016.
18. Pavone, S. C., M. Ettorre, and M. Albani, "Analysis and design of Bessel beam launchers: Longitudinal polarization," *IEEE Trans. Anten. Propag.*, Vol. 22, No. 6, 2311–2318, 2016.
19. Pavone, S. C., A. Mazinghi, A. Freni, and M. Albani, "Comparison between broadband Bessel beam launchers based on either Bessel or Hankel aperture distribution for millimeter wave short pulse generation," *Opt. Expr.*, Vol. 25, No. 16, 19548–19560, 2017.
20. Comite, D., W. Fuscaldo, S. C. Pavone, et al., "Propagation of nondiffracting pulses carrying orbital angular momentum at microwave frequencies," *Appl. Phys. Lett.*, Vol. 110, No. 11, 114102, 2017.
21. Mazinghi, A., A. Freni, A. Agostini, L. Bossio, and M. Albani, "Industrial antenna development for 77 GHz level-crossing monitoring radar," *IEEE Antennas Propag. Magaz.*, Vol. 60, No. 5, 95–106, 2018.
22. Iigusa, K., K. Li, K. Sato, and H. Harada, "Gain enhancement of H -plane sectoral post-wall horn antenna by connecting tapered slots for millimeter-wave communication," *IEEE Trans. Antennas Propag.*, Vol. 60, No. 12, 5548–5556, 2012.
23. Olver, A. D., P. J. B. Clarricoats, et al., *Microwave Horns and Feeds*, No. 39, IET, 1994.
24. Weily, A. R., K. P. Esselle, T. S. Bird, and B. C. Sanders, "Linear array of woodpile EBG sectoral horn antennas," *IEEE Trans. Antennas Propag.*, Vol. 54, No. 8, 2263–2274, 2006.
25. Pavone, S. C., A. Mazinghi, and M. Albani, "PO-based automatic design and optimization of a millimeter wave sectoral beam shaped reflector," *IEEE Trans. Antennas Propag.*, 2020, doi: 10.1109/TAP.2020.2971523.
26. Elliott, R. S., "The design of waveguide-fed slot arrays," chap. in Y. T. Lo, S. W. Lee, *Antenna Handbook*, Springer, 1988.
27. Bakhtafrooz, A., A. Borji, D. Busuioc, and S. Safavi-Naeini, "Novel two-layer millimeter-wave slot array antennas based on substrate integrated waveguides," *Progress In Electromagnetics Research*, Vol. 109, 475–491, 2010.
28. Sekretarov, S. and D. M. Vavriv, "A wideband slotted waveguide antenna array for SAR systems," *Progress In Electromagnetics Research M*, Vol. 11, 165–176, 2010.
29. Mondal, M. and A. Chakraborty, "Parametric study of waveguide slots and analysis of radiation pattern for the design of waveguide array antenna," *Progress In Electromagnetics Research M*, Vol. 4, 93–103, 2008.
30. Balanis, C. A., *Advanced Engineering Electromagnetics*, John Wiley & Sons, 2012.